Dynamic Behavior of Variable Stroke Swash Plate Mechanism*

Katsutoshi YOSHIDA**, Kohju KASAHARA** and Shinichi WATANABE***
** Department of Mechanical Systems Engineering, Faculty of Engineering, Utsunomiya University
7-1-2, Yoto, Utsunomiya, Tochigi, 321-8585, Japan
E-mail: yoshidak@cc.utsunomiya-u.ac.jp
*** Innovation Center for Research and Engineering Education, Utsunomiya University
7-1-2, Yoto, Utsunomiya, Tochigi, 321-8585, Japan
E-mail: swtnb@cc.utsunomiya-u.ac.jp

Abstract
Dynamic behavior of a variable stroke swash plate mechanism is analytically and numerically investigated. Deriving a simple degree of freedom model, we propose a dimensionless arm length to characterize dynamic stabilities of the swash plate angle. We then make a comparison between two types of constraints of the swash plate: one fixating the plate with the swing component and the other linking it with the followers in a frictionless manner. It is numerically shown that the fixed-type constraint improves the stabilities of the mechanism while the frictionless-type constraint makes the mechanism destabilized. An equivalent design technique is also proposed to convert optimal specifications between the different types of the constraints.

Key words : Swash Plate, Rotor, Stability, Constraint, Equivalent Design.

1. Introduction

Variable stroke swash plate mechanisms provide a key technology of controlling flows or pressures of axial piston compressors that can vary its displacement by changing the swash plate angle. Zeiger and Akers(1) derived linearized equations of the system's state of a variable displacement swash plate axial piston pump to evaluate the torque on the swash plate about its pivot. A closed-form expression of the dynamic equations was developed by Manring and Johnson(2) to provide several simple equations for designing the control gain of the pump. Zhang et al.(3) improved the model to represent the damping mechanism of the swash plate angle analytically. Tain et al.(4) developed the steady-state mathematical model of the variable displacement swash plate compressor by combining the force balance equation and the mass and energy conservation equation. It seems that main interest of these studies was in performance control of the compressors. Since their models are linearized or simplified, they are not suitable for understanding nonlinear dynamics of the mechanisms such as geometric nonlinearity generated by rigid rotors.

In this paper, we investigate the nonlinear dynamics of the variable stroke swash plate mechanism regarding it as a rigid rotor. We derive a simple degree of freedom model of the swash plate angle to consider two types of constraints of the swash plate. We characterize constraint-induced dynamic instability arising in the swash plate mechanism through the use of bifurcation diagrams.

2. Kinematics

Figure 1 shows the free-body diagram of the swash plate. We first lay the disk horizontally, putting the pivot (denoted as A) along y-axis. From this initial configuration, the swash plate (disk) spins along z-axis over the angle ψ, then swings along x-axis over the angle θ, and finally rotates along z-axis over the angle ϕ. The cum follower (denoted as P) is linked with

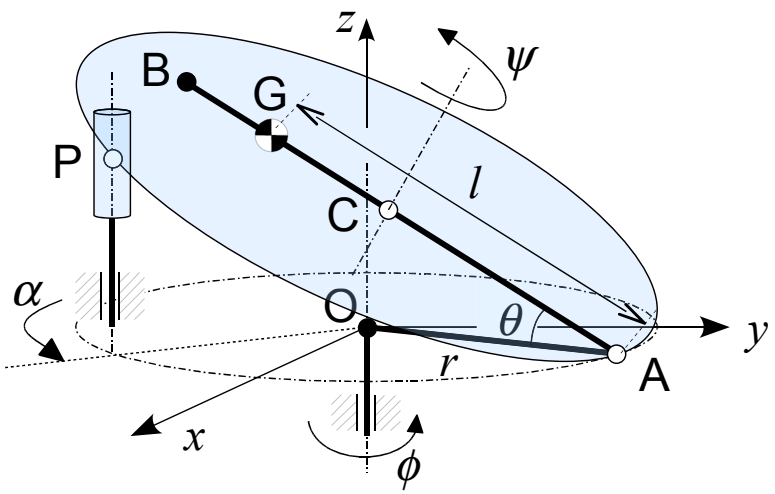

Fig. 1 Free-body diagram of the swash plate.

the swash plate and can move along vertical line placed at (r, α) by polar coordinate system in the xy-plane. We regard the three angles (ϕ, θ, ψ) as the generalized coordinates of our problem.

In what follows, we refer to ϕ as in input shaft angle, θ as a swash plate angle, and ψ as a spin angle. Unit vectors along x, y, and z-axis are denoted as $\boldsymbol{i}$, $\boldsymbol{j}$, $\boldsymbol{k}$ respectively. Furthermore, rotational transformations along x and z-axis are represented as $R_x(\cdot)$ and $R_z(\cdot)$ respectively, and E denotes the identical transformation.

2.1. Swash plate kinematics

From Fig. 1, the position vector $\boldsymbol{X}_G$ of the center-of-mass G of the swing component supporting the swash plate is expressed as

$$\boldsymbol{X}_G = R_z(\phi)\big(rE - lR_x(-\theta)\big)\boldsymbol{j} = \begin{pmatrix} (l\cos\theta - r)\sin\phi \\ -(l\cos\theta - r)\cos\phi \\ l\sin\theta \end{pmatrix} \tag{1}$$

and the angular velocity of the swash plate is of the form:

$$\boldsymbol{\omega} = -\dot{\theta}R_z(\phi)\boldsymbol{i} + \big(\dot{\phi}E + \dot{\psi}R_z(\phi)R_x(-\theta)\big)\boldsymbol{k} = \begin{pmatrix} -\dot{\theta}\cos\phi - \dot{\psi}\sin\phi\sin\theta \\ -\dot{\theta}\sin\phi + \dot{\psi}\cos\phi\sin\theta \\ \dot{\phi} + \dot{\psi}\cos\theta \end{pmatrix} \tag{2}$$

From these vectors, the total kinetic energy of the swash plate component is obtained as follows.

$$\begin{aligned} T_S &= \frac{m_G}{2}\dot{\boldsymbol{X}}_G^2 + \frac{1}{2}\boldsymbol{\omega}\cdot\big(J\boldsymbol{\omega}\big) \\ &= \frac{J_1}{2}\big(\dot{\phi}^2\sin^2\theta + \dot{\theta}^2\big) + \frac{J_3}{2}\big(\dot{\phi}\cos\theta + \dot{\psi}\big)^2 + \frac{m_G}{2}\big(\dot{\phi}^2(l\cos\theta - r)^2 + l^2\dot{\theta}^2\big) \end{aligned} \tag{3}$$

where m_G is a mass of the swing component and $J = \mathrm{diag}\{J_1, J_1, J_3\}$ is a inertia tensor of the swash plate with respect to the initial configuration $(\phi, \theta, \psi) = \boldsymbol{0}$. We assume $J = \rho\,\mathrm{diag}\{1, 1, 2\}$ regarding that the thickness of the swash plate is neglectable.

2.2. Cum follower kinematics

We make the following assumptions about the cum follower kinematics:

(H1) The distance between the rotation axis (z-axis) and the cum follower axis (parallel to z-axis) is identical to r.

(H2) The cum follower is at bottom dead center when the pivot (A) crossing the cum follower axis.

Then, the center-of-mass vector of the i-th cum follower can be written as

$$\boldsymbol{P}_i = r\begin{pmatrix}\cos\alpha_i \\ \sin\alpha_i \\ -(n_1\cos\alpha_i + n_2\sin\alpha_i)n_3^{-1}\end{pmatrix} - \begin{pmatrix}0\\0\\h\end{pmatrix} \tag{4}$$

where $\boldsymbol{n} = (n_1, n_2, n_3) = (-\sin\phi\sin\theta, \cos\phi\sin\theta, \cos\theta)$ is a normal vector of the swash plate, α_i is a position angle of the ith cum follower, and h is a position of the bottom dead center of the cum followers. Assuming the cum follower axes being placed uniformly, we have

$$\alpha_i = \frac{2\pi(i-1)}{n} \quad (n = 1, 2, \cdots, n) \tag{5}$$

where n is the number of the cum followers. Therefore, the total kinetic energy of the n cum followers is obtained as

$$T_P = \sum_{i=1}^{n}\frac{m_P}{2}\dot{\boldsymbol{P}}_i^2 = n\cdot\frac{m_P r^2}{4}\left(3\dot\theta^2\sec^4\theta + \dot\phi^2\tan^2\theta\right) \tag{6}$$

where m_P is the mass of the cum follower.

2.3. External forcing

We model the external components outside of the swash plate cum mechanism as the n external forces $F_1, F_2, \cdots, F_n \in \mathrm{R}$ parallel to the z-axis where the ith force F_i is applied to the ith cum follower. The generalized forces of our problem are thus expressed as

$$\begin{pmatrix}F_\phi\\F_\theta\\F_\psi\end{pmatrix} = r\sum_{i=1}^{n}F_i\begin{pmatrix}\cos(\phi-\alpha_i)\tan\theta\\\left(1+\sin(\phi-\alpha_i)\right)\sec^2\theta\\0\end{pmatrix}. \tag{7}$$

In practice, the external force F_i would be piston pressures in the application of variable displacement swash plate compressors for automotive air conditioning system.

3. Analytical Model

3.1. Equation of motion (EOM)

From Equations (3) and (6), the Lagrange function L of the variable stroke swash plate cum mechanism with the cum followers is obtained as

$$\begin{aligned}L =& T_S + T_P \\ =& \left(J_1\sin^2\theta + J_3\cos^2\theta + m_G(l\cos\theta - r)^2 + n\cdot\frac{m_P r^2}{2}\tan^2\theta\right)\frac{\dot\phi^2}{2} \\ &+ \left(J_1 + m_G l^2 + n\cdot\frac{m_P r^2}{\sec^4\theta}\right)\frac{\dot\theta^2}{2} + J_3\frac{\dot\psi^2}{2} + (J_3\cos\theta)\dot\phi\dot\psi.\end{aligned} \tag{8}$$

From Equations (7) and (8), the EOM of the mechanism is derived as

$$\begin{pmatrix}M_1(\theta) & 0 & J_3\cos\theta\\ 0 & M_2(\theta) & 0\\ J_3\cos\theta & 0 & J_3\end{pmatrix}\begin{pmatrix}\ddot\phi\\\ddot\theta\\\ddot\psi\end{pmatrix} = \sin\theta\begin{pmatrix}2H(\theta)\dot\theta\dot\phi + J_3\dot\theta\dot\psi\\ -H(\theta)\dot\phi^2 - 6J_P(\theta)\dot\theta^2\sec\theta - J_3\dot\phi\dot\psi\\ -J_3\dot\theta\dot\phi\end{pmatrix} + \begin{pmatrix}F_\phi\\F_\theta\\F_\psi\end{pmatrix} \tag{9}$$

where $A = \rho + m_G l^2$, $A^* = A + \rho$, $B = m_G rl$, $M_P(\theta) = n(m_p r^2/2)\sec^4\theta$, $M_1(\theta) = m_G r^2 - 2B\cos\theta + J_1\sin^2\theta + (A^* + M_P(\theta)\sin^2\theta)\cos^2\theta$, $M_2(\theta) = A + 3M_P(\theta)$, and $H(\theta) = (A - M_P(\theta))\cos\theta - B$.

3.2. Reduced order model

Suppose that the input angle ϕ does not depends on the other state variables of the mechanism. Namely, we make the following assumption:

(H3) The input shaft velocity $\dot{\phi}$ is given by some known function $\dot{\phi} = \omega(t)$.

(H4) The spin velocity $\dot{\psi}$ can be expressed as $\dot{\psi} = -\delta\dot{\phi}$ ($\delta = 0, 1$) corresponding to two types of constraints being imposed on the spin angle.

The condition $\delta = 0$ means that the swash plate disk is fixed to the swing component, in other words, there is no relative motion between the disk and the swing component. On the other hand, the condition $\delta = 1$ means that the swash plate disk can not spin around z-axis, and the disk is linked with the cum follower components while it can slip around the input shaft in a frictionless manner. Reducing the EOM (9) with respect to the accelerations and applying (H3) and (H4), we have a simple degree of freedom EOM of the form:

$$M_2(\theta)\ddot{\theta} + 6\dot{\theta}^2 \tan\theta + \omega^2\Big(H(\theta) - \delta J_3\Big)\sin\theta = F_\theta$$

Adding the linear damping force $c\dot{\theta}$ and the linear bias spring force $k(\theta - \bar{\theta})$ to the expression above, we obtain the reduced-order model of the variable stroke swash plate cum mechanism:

$$M_2(\theta)\ddot{\theta} + 6\dot{\theta}^2 \tan\theta + \omega^2\Big(H(\theta) - \delta J_3\Big)\sin\theta = F_\theta - c\dot{\theta} - k(\theta - \bar{\theta}) \tag{10}$$

where $\bar{\theta}$ is the static equilibrium of the swash plate angle.

4. Stability of Free Motion

It is clearly seen from Equation (10) that the swash plate mechanism is basically expressed by nonlinear differential equations due to geometric and kinematic nonlinearities of the mechanism. From this reason, in previous studies[(1)−(4)], the original equations of motion of the mechanism are linearized or simplified because they prefer simpler dynamic models to investigate effects of the external forcing F_θ in detail where the forcing is expected to represent the piston pressures of the swash plate compressors and so on. Therefore, it seems that dynamical effects of the nonlinearity have not been fully understood yet.

As another approach to the simplification, in this paper, we ignore effects of the cum followers (or pistons) to maintain the geometric and kinematic nonlinearity of the mechanism. Supposing that $M_P(\theta) = F_\theta = 0$ to remove the dynamic effects of the cum followers, we obtain a simpler expression of the free motion of the swash plate mechanism in the following form:

$$A\ddot{\theta} + \omega^2\Big(A\cos\theta - B - \delta J_3\Big)\sin\theta + c\dot{\theta} + k(\theta - \bar{\theta}) = 0 \tag{11}$$

4.1. Dimensionless Arm Length

Dimensionless form of Equation (11) provides a useful criterion for equivalent design of the variable stroke swash plate mechanism having different constraints. Applying the time scale transformation $t \mapsto \nu t$, and dividing by $A\nu^2$, Equation (11) is rewritten as

$$\ddot{\theta} + \omega^2\left(\frac{A\cos\theta - B - \delta J_3}{A\nu^2}\right)\sin\theta + \frac{c}{A\nu}\dot{\theta} + \frac{k}{A\nu^2}(\theta - \bar{\theta}) = 0.$$

Then, choosing the time scale ν satisfying $A\nu^2 = B + \delta J_3$ and putting

$$\begin{aligned} C_\delta &= c(A\nu)^{-1} = c((\rho + m_G l^2)(\delta\cdot 2\rho + m_G r l))^{-1/2}, \\ K_\delta &= k(A\nu^2)^{-1} = k(\delta\cdot 2\rho + m_G r l)^{-1}, \\ \Lambda_\delta &= \nu^{-2} = (\rho + m_G l^2)(\delta\cdot 2\rho + m_G r l)^{-1}, \end{aligned} \tag{12}$$

we have the dimensionless form of Equation (11):

$$\ddot{\theta} + \omega^2(\Lambda_\delta\cos\theta - 1)\sin\theta + C_\delta\dot{\theta} + K_\delta(\theta - \bar{\theta}) = 0. \tag{13}$$

We refer to the dimensionless parameters $C_\delta, K_\delta, \Lambda_\delta$ as a dimensionless damping, spring stiffness, and arm length, respectively.

The dimensionless arm length (DAL) Λ_δ governs stability of the unperturbed trivial solution of the swash plate dynamics (13). To see that, substituting the unperturbed condition $c = k = 0$ and its trivial solution $\theta = 0$ into the first variation equation of (13) given by

$$\ddot{\xi} + \omega^2(\Lambda_\delta \cos 2\theta - \cos\theta)\xi + C_\delta\dot{\xi} + K_\delta\xi = 0,$$

then, we have $\ddot{\xi} + \omega^2(\Lambda_\delta - 1)\xi = 0$. This proves the following proposition.

- The unperturbed trivial solution $\theta = 0$ of the dimensionless EOM (13) is stable if $\Lambda_\delta > 1$ and is unstable if $\Lambda_\delta < 1$.

This proposition holds even in the perturbed case $c, k \neq 0$ near $\theta = 0$ when the input angular velocity ω is sufficiently large.

It is worth noting that the dimensionless form (13) coincides with the point-mass approximation ($\rho = 0$) of (11) with the unit mass and radius ($m_G = r = 1$), given by

$$\ddot{\theta} + \omega^2(l\cos\theta - 1)\sin\theta + c\dot{\theta} + k(\theta - \bar{\theta}) = 0. \tag{14}$$

This means that all the changes in physical dimensions of the swash plate mechanism including the types of constraints are renormalized into the point-mass approximated coefficients: $C_\delta \mapsto c$, $K_\delta \mapsto k$, and $\Lambda_\delta \mapsto l$, in equation (14).

In this context, a physical explanation of Λ_δ can easily be obtained as follows. The unperturbed trivial solution of the mechanism is stabilized by the centrifugal force when the arm length l extends beyond the radius r (= 1) while it is destabilized by the centrifugal force in the opposite direction when the arm length l can not reach the input shaft axis.

4.2. Constraint-induced Instability of the Swash Plate Mechanism

The simplest application of the DAL Λ_δ is characterizing how the dynamic stability of the mechanism depends on the constraint parameter δ. For simplicity, we regard the point-mass approximation (14) under the unperturbed assumption $k = c = 0$ with the unit mass and radius ($m_G = r = 1$) as a reference model. The reference model has a neutrally stable trivial solution at $\theta = 0$ when the physical arm length l is designed to coincide with the physical radius r (as discussed in section 4.1). In this unperturbed case, the DAL equals unity:

$$\Lambda_\delta = \frac{0 + m_G l^2}{\delta \cdot 2 \cdot 0 + m_G l l} = \frac{m_G l^2}{m_G l^2} = 1. \tag{15}$$

Under the same geometric setup, restoring the volume of the rigid body $\rho \neq 0$, we can show that the constraint parameter $\delta = 0, 1$ changes the stability of the trivial solution $\theta = 0$.

Provided $\delta = 0$, i.e. the swash plate disk is fixed with the swing component (drawn as AB in Fig. 1), we have the DAL greater than unity:

$$\Lambda_0 = \frac{\rho + m_G l^2}{0 \cdot 2\rho + m_G l l} = \frac{\rho + m_G l^2}{m_G l^2} > 1. \tag{16}$$

This means that restoring the volume of the reference model with the fixed constraint increases the DAL to improve the stability of the trivial solution. On the other hand, the frictionless constraint $\delta = 1$ between the swash plate disk and the swing component results in

$$\Lambda_1 = \frac{\rho + m_G l^2}{1 \cdot 2\rho + m_G l l} = \frac{\rho + m_G l^2}{2\rho + m_G l^2} < 1. \tag{17}$$

This means that restoring the volume with the frictionless constraint decreases the DAL to destabilize the trivial solution.

From these results, it is clearly shown that the geometric design with the ratio $l/r = 1$ does not match the dynamic design with $\Lambda_\delta = 1$. This implies that there are multiple geometric designs dynamically equivalent to each other. For example, it is possible to derive a dynamically equivalent design between the two constraints mentioned above. In practice,

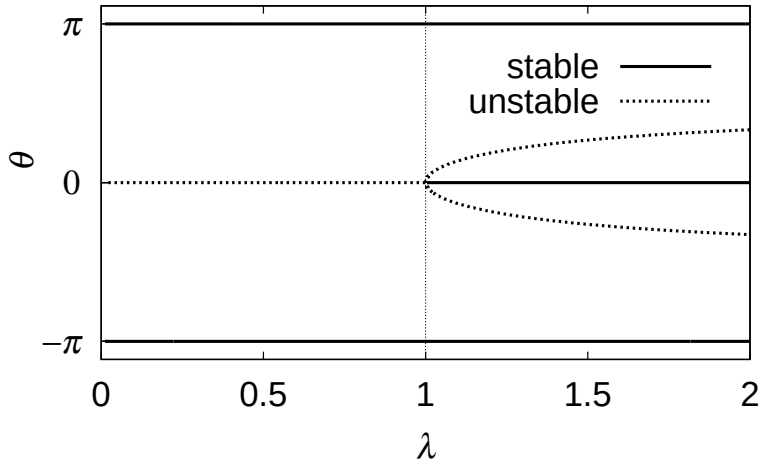

Fig. 2 Bifurcation diagram of the swash plate angle θ with respect to the geometric ratio λ under the point-mass approximation $\rho = 0$ and without the bias spring $k = 0$. The subcritical pitchfork bifurcation occurs.

an unknown physical arm length l_δ can be determined from a given specification $\Lambda_\delta = \tilde{\Lambda}$. Solving the relation: $\Lambda_\delta = (\rho + m_G l^2)(\delta \cdot 2\rho + m_G r l)^{-1} = \tilde{\Lambda}$, we have the following formula:

$$l_\delta = \frac{r\tilde{\Lambda} \pm \sqrt{(r\tilde{\Lambda})^2 + 4\rho m_G^{-1}(2\delta\tilde{\Lambda} - 1)}}{2} \tag{18}$$

which enables us to determine the physical arm length l_δ satisfying the specification $\tilde{\Lambda}$.

4.3. Bifurcation Diagram

Table 1 summarizes specifications typical of variable displacement swash plate compressors for automotive air conditioning system of the maximal displacement about 150 cc/rev. We empirically select the other parameters $c = 0.2$, $k = 2$. We refer to the ratio $\lambda := l/r$ as a geometric ratio of the mechanism in what follows.

Table 1 Specifications typical of variable displacement swash plate compressors for automotive air conditioning system of the maximal displacement about 150 cc/rev.

Parameter	Value	Parameter	Value
m_G	0.5 kg	$\lambda := l/r$	0.9 to 1.1
ρ	1.5×10^{-4} kgm^2	Λ_0	1.172 to 1.323
r	3.5×10^{-2} m	Λ_1	0.759 to 0.915

Under these conditions and the point-mass approximation $\rho = 0$, Fig. 2 shows the unperturbed bifurcation diagram of the swash plate angle θ with respect to the geometric ratio λ without the bias spring $k = 0$. In this case, the geometric ratio $\lambda = 1$ corresponds to $\Lambda_\delta = 1$ and produces the neutrally stable equilibrium at $\theta = 0$ as already proven by equation (15). It is clear from Fig. 2 that this unperturbed condition is characterized by the subcritical pitchfork bifurcation occurring at $\lambda = 1$.

Figure 3 shows that as restoring the rigid body volume to $\rho = 1.5 \times 10^{-4}$ kgm^2 under the fixed constraint $\delta = 0$, the pitchfork bifurcation point shifts to the left-hand side and the second subcritical pitchfork bifurcation occurs at left-hand side of the first point. This means that the neutrally stable solution $\theta = 0$ under the geometry $\lambda = 1$ is stabilized by the fixed constraint $\delta = 0$ and consequently by the larger DAL $\Lambda_0 > 1$ as discussed in equation (16). It can be easily clarified that Λ_0 is less than unity between the bifurcation points at $\lambda \approx 0.429$, 0.572 and it takes the minimal value at $\lambda \approx 0.495$ which is represented as unstable dotted line segment between the bifurcation points.

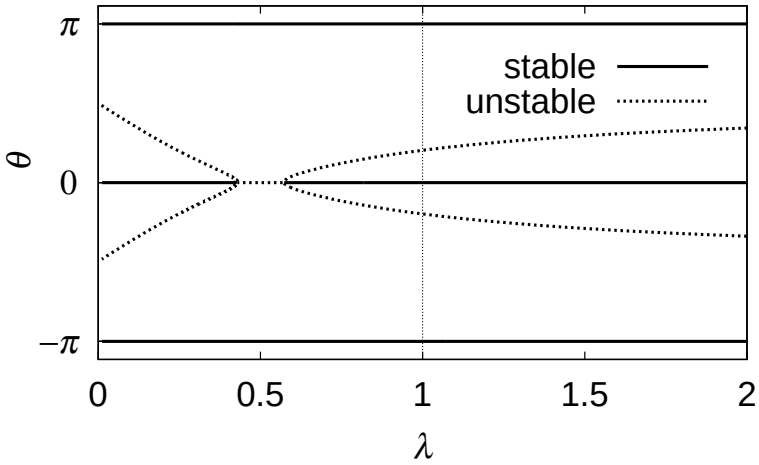

Fig. 3 Bifurcation diagram of the swash plate angle θ with respect to the geometric ratio λ for $\rho = 1.5 \times 10^{-4}$ and $k = 0$ under the fixed constraint $\delta = 0$. The bifurcation point has shifted to left-hand side and the second point of subcritical pitchfork bifurcation appears at $\lambda \approx 0.429$.

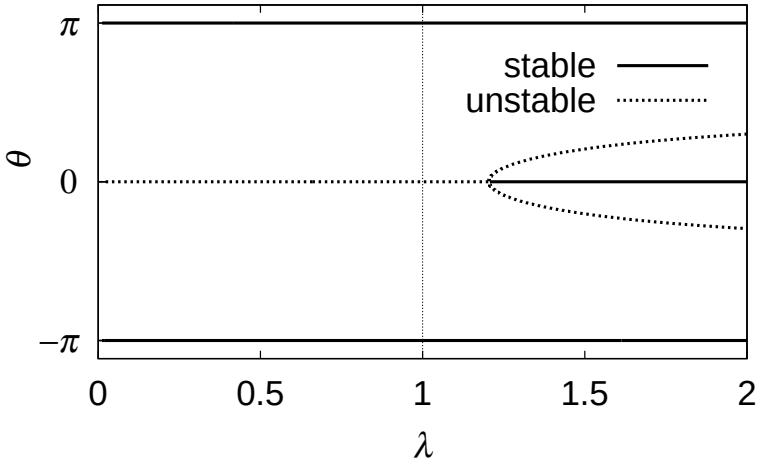

Fig. 4 Bifurcation diagram of the swash plate angle θ with respect to the geometric ratio λ for $\rho = 1.5 \times 10^{-4}$ and $k = 0$ under the frictionless constraint $\delta = 1$. The bifurcation point has shifted to right-hand side.

On the other hand, as shown in Fig. 4, under the frictionless constraint $\delta = 1$, the bifurcation point shifts in the opposite direction. Consequently, the neutrally stable solution $\theta = 0$ under the geometry $\lambda = 1$ is destabilized by the frictionless constraint resulting in the smaller DAL $\Lambda_1 < 1$ as discussed in equation (17).

These bifurcation diagrams provide detailed explanation of the presence of constraint-induced instability of the swash plate mechanism. It is shown that the neutrally stable solution $\theta = 0$ under the geometry $\lambda = 1$ is stabilized by the fixed constraint $\delta = 0$ while it is destabilized by the frictionless constraint $\delta = 1$.

In industrial applications, however, some bias restoring force on θ (represented as $k \neq 0$ in our case) must be applied in order to maintain the designed or controlled swash plate angle θ (or stroke). Such a restoring force would be generated by mechanical springs or certain feedback controllers. In such a case, the pitchfork bifurcations observed above are perturbed to saddle node bifurcations. Figure 5 shows the simplest example of how the pitchfork bifurcation in Fig. 2 is perturbed simply by adding the bias spring of $k = 2$, $\bar{\theta} = \pi/9$.

Figures 6 and 7 represent the more general condition where the system is perturbed by both the nonzero volume of $\rho = 1.5 \times 10^{-4}$ and the bias spring of $k = 2$, $\bar{\theta} = \pi/9$. The diagrams are plotted with respect to the input angular velocity ω in this case. Figure 6 shows the result

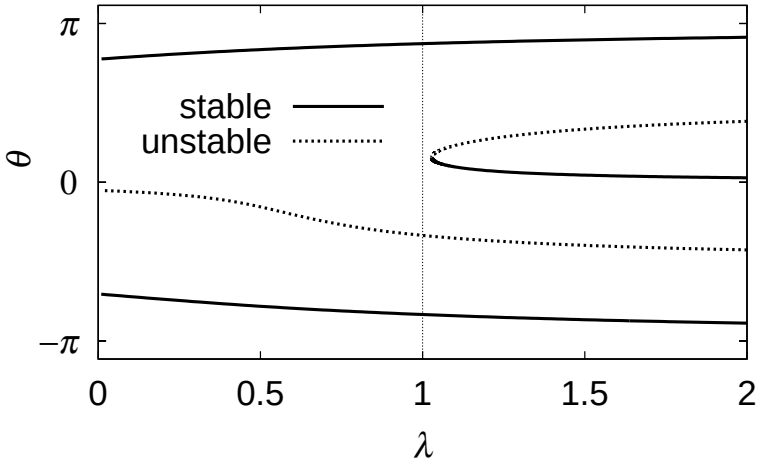

Fig. 5 Perturbed bifurcation diagram with the bias spring, $k = 2 \neq 0$, with respect to λ under the point-mass approximation $\rho = 0$. The pitchfork bifurcation in Fig. 2 is perturbed to the saddle-node bifurcation.

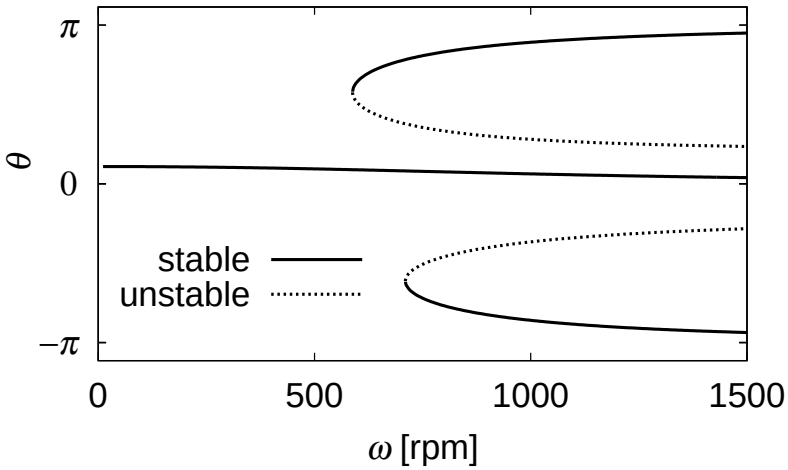

Fig. 6 General bifurcation diagram of the swash plate angle θ with respect to the input angular velocity ω under the fixed constraint $\delta = 0$.

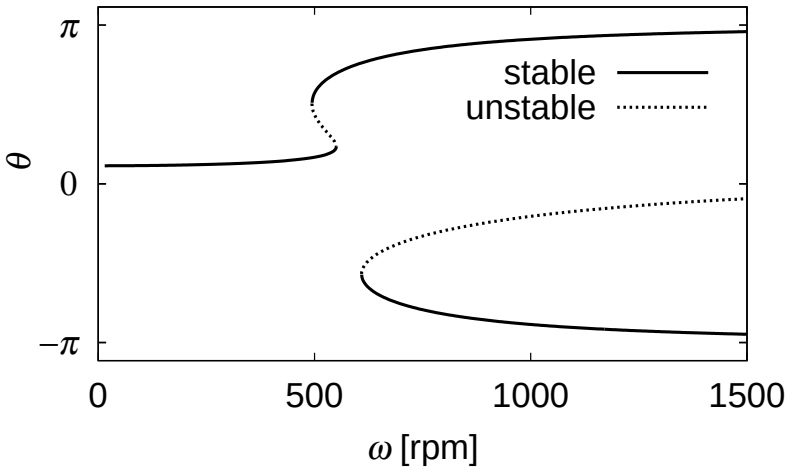

Fig. 7 General bifurcation diagram of the swash plate angle θ with respect to the input angular velocity ω under the frictionless constraint $\delta = 1$. The stable branch near $\theta = 0$ disappears for sufficiently large ω.

for the fixed constraint $\delta = 0$ and Fig. 7 for the frictionless constraint $\delta = 1$ respectively. In addition, it is worth noting that in practical situations, the displacement of the swash plate angle θ is limited from $\theta = 0$ to less than about $\pi/6$ rad (= 30 deg) so that it is enough to focus on the branches near $\theta = 0$ from the engineering viewpoint.

Even in these general situations, it can still be concluded that the constraint-induced instability may arise though it appears only at high speed region $\omega > 609$ rpm. In practice, it is clear from Figs. 6 and 7 that the stable equilibrium near $\theta = 0$ for the fixed constraint ($\delta = 0$) vanishes at the high speed region as the constraint changes from the fixed type $\delta = 0$ to the frictionless type $\delta = 1$.

5. Conclusion

The nonlinear equation of motion of the variable stroke swash plate mechanism has been derived to obtain the simple degree of freedom model of the geometrically nonlinear motion of the swash plate angle θ. To characterize the stabilities of the mechanism, we have introduced the dimension less arm length (DAL) and investigated the constraint-induced dynamic instability of the mechanism. The obtained results are summarized as follows.

(1) The large class of the free motion of the mechanism can be renormalized into the simplest model of the point-mass formalism.

(2) The unperturbed solution is stabilized by the fixed constraint $\delta = 0$ and destabilized by the frictionless constraint $\delta = 1$.

(3) The general perturbed solution at high speed region $\omega \gg 1$ rpm also loses its stabilities as the constraint changes from the fixed type $\delta = 0$ to the frictionless type $\delta = 1$.

(4) The two types of constraints can be dynamically equivalent to each other under the proposed design formula (18).

The above result leads to the conclusion that the dynamics of the variable stroke swash plate mechanism can not be understood without considering the geometric and kinematic nonlinearity generated by the rigid rotors with the constraints.

Acknowledgments

Gratitude is expressed to Calsonic Kansei Corporation Technical Center in Tochigi for furnishing the geometric data and for helpful discussions.

References

(1) G. Zeiger and A. Akers, Torque on the Swashplate of an Axial Piston Pump, ASME Journal of Dynamic Systems, Measurement, and Control, Volume 102, 1985, pp.220-226.

(2) N. D. Manring and R. E. Johnson, Modeling and Designing a Variable-Displacement Open-Loop Pump, ASME Journal of Dynamic Systems, Measurement, and Control, Volume 118, 1996, pp.267-271.

(3) X. Zhang, J. Cho, S. S. Nair and N. D. Manring, New Swash Plate Damping Model for Hydraulic Axial-Piston Pump, ASME Journal of Dynamic Systems, Measurement, and Control, Volume 123, 2001, pp.463-470.

(4) Changqing Tain, Yunfei Liao and Xianting Li, A mathematical model of variable displacement swash plate compressor for automotive air conditioning system, International Journal of Refrigeration, Volume 29, 2006, 270-280.